# Role of the Electron Spin Polarization in Water Splitting

Wilbert Mtangi,[†] Vankayala Kiran,[†] Claudio Fontanesi,[†,‡] and Ron Naaman[*,†]

[†]Department of Chemical Physics, Weizmann Institute of Science, Rehovot 76100, Israel

[‡]Department of Engineering 'Enzo Ferrari', Universita' degli Studi di Modena e Reggio Emilia, Via Vivarelli 10 41125 Modena, Italy

S *Supporting Information*

ABSTRACT: We show that in an electrochemical cell, in which the photoanode is coated with chiral molecules, the overpotential required for hydrogen production drops remarkably, as compared with cells containing achiral molecules. The hydrogen evolution efficiency is studied comparing seven different organic molecules, three chiral and four achiral. We propose that the spin specificity of electrons transferred through chiral molecules is the origin of a more efficient oxidation process in which oxygen is formed in its triplet ground state. The new observations are consistent with recent theoretical works pointing to the importance of spin alignment in the water-splitting process.
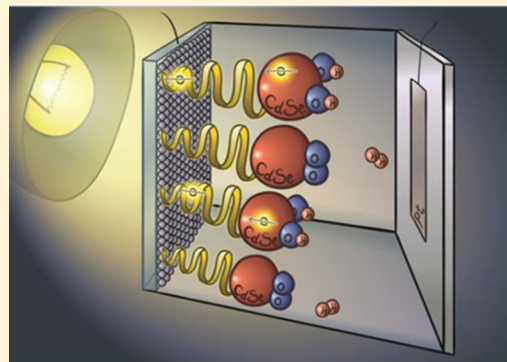
Hydrogen production from water by (photo) electrochemical cells is an example of multiple electrons reactions. The practical production of hydrogen from water in an efficient way is hampered by the need to supply an external voltage (over potential) to initiate the reaction.[1-7] Hence, although hydrogen is considered to be the ultimate fuel of the future, its efficient production remains a challenge.[8-11] Recently, theoretical studies have suggested that the overpotential required to split water into hydrogen and oxygen stems from electrons' spin restrictions in forming the ground-state triplet oxygen molecule.[12] When nonmagnetic electrodes are used, the reaction involves contribution from the singlet potential surface, which correlates with the excited state of oxygen, and hence a barrier exists. It has been proposed that magnetic electrodes, in which the electrons spins are coaligned, might overcome this problem;[13] however, magnetic electrodes introduce new challenges, both economically and technologically. Here we managed to overcome the spin-restriction problem by introducing anodes coated with chiral molecules. Indeed, we observed a significant reduction in the overpotential required for hydrogen production. This observation can be explained by the spin-selective electron conduction through these chiral molecules.[14,15] This finding on the one hand opens the way for efficient production of hydrogen and on the other hand points to the possible importance of chirality and spin selectivity in multiple electron reactions in biology. In the present study, two different cell configurations for hydrogen production were tested; in both, the chiral-molecule effect was verified. The efficiency of these chiral molecules as spin filters was correlated with the reduction in the overpotential measured in cells where the anode is coated with them.

We use photoanodes functionalized with chiral molecules. At the photoanode, oxygen molecules in their triplet ground state are formed. In the process, four electrons are transferred. The formation of the triplet requires a specific spin correlation between the transferred electrons. This issue has been intensively debated for the similar bioprocess of oxygen formation by photosystem II.[16-19] The detailed mechanism underlying the final stage of the O–O bond formation and O_2 evolution remains unsettled despite extensive theoretical studies and will not be discussed here.[20-23]

The chiral-induced spin selectivity (CISS) effect,[14,15] discovered in recent years, indicates that molecular chirality and the spin of electrons transported through these molecular systems are correlated. Moreover, it was found that electrons transferred through photosystem I are spin polarized.[24] This spin polarization may provide the required spin correlation between the electrons transferred from the oxygen/sulfur atoms into the holes in the semiconducting electrode. It will be shown here that by using chiral molecules for electron transfer it is indeed possible to lower the overpotential for hydrogen production.

■ EXPERIMENTAL METHODS

Preparation of TiO_2 Electrodes. TiO_2 nanoparticulate films were deposited on fluorine-doped tin oxide (FTO, surface resistivity of ~7 Ω/sq) coated glass, purchased from Sigma-Aldrich, using the electrophoretic deposition (EPD) technique. This technique has been previously used to deposit uniform TiO_2 films.[25-29] A suspension of TiO_2 nanoparticles (NPs) was prepared by dispersing 0.4 g TiO_2 NP (<25 nm in diameter and 99.7% trace metals, from Sigma-Aldrich) in 40 mL of deionized water. Prior to making dispersions, TiO_2 nanoparticle powders

were heated at 300 °C for 1 h. The mixture was stirred overnight to ensure homogeneity. Prior to nanoparticle deposition, the FTO substrates were boiled in isopropanol for 15 min, followed by 15 min of boiling in ethanol and finally rinsed with deionized water. After having been rinsed, the substrates were dried using nitrogen gas and annealed for 15 min at T = 570 K. EPD was then performed with a Princeton potentiostat using the galvanic pulses mode technique with two pulses (Pulse 1 and Pulse 2).

Pulse 1 was set to 0 mA for 200 s for depolarization. Pulse 2 has current values ranging from 0.50 to 0.95 mA (producing a maximum potential of 7.0 V). Pulse 2 was applied for 1000 s in each cycle for polarization, and the number of iterations (pulse 1 followed by pulse 2) was set to 750. Various cycles were used to prepare films of required thicknesses. The samples were annealed in between cycles at 570 K for 15 min in air. During EPD, the suspension was continuously stirred using a magnetic stirrer. After completion of the last cycle, the electrodes were annealed again for 8 h.

To confirm the surface coverage of the EPD-deposited TiO_2 NP on FTO, high-resolution scanning electron microscope (SEM) measurements were performed using In-lens-detector imaging with a LEO-Supra 55 VP. The SEM images in Figure S1 show a high surface coverage of the TiO_2 NP on FTO substrates deposited using the EPD technique. An average film thickness of ~6.8 μm was measured using the Dektak stylus profilometer.

Functionalization of the Electrode by the Linker Molecules. TiO_2 films were functionalized using organic linker molecules in order to attach the CdSe NP. In this study, (COOH)-(Ala-Aib)$_5$-NH-(CH$_2$)$_2$-SH (Al5), (COOH)-(Ala-Aib)$_7$-NH-(CH$_2$)$_2$-SH (Al7), 11-mercapto-undecanoic acid (MUA), 3-mercaptobenzoic acid (3 MBA), 4-mercaptobenzoic acid (4 MBA), and 3-mercaptopropionic acid (MPA) were used as linkers. The oligopeptide was dissolved in dimethylformamide (DMF) to afford a 0.10 mM solution, whereas MPA and MUA were dissolved in ethanol to afford 5 and 1 mM solutions, respectively. 3 MBA and 4 MBA were also dissolved in ethanol to afford 1 mM solutions. The 1.0×1.5 cm^2 electrodes coated with TiO_2 were then immersed into the linker molecule solutions for an incubation period of 48 h. The linker molecules are attached to the TiO_2 surface by their carboxylic group.[30−32]

Modification of Electrodes with dsDNA. We used single-stranded DNA, a 40-base oligonucleotide (40 bp) with the following sequence: 5′-AAA GAG GAG TTG ACA GTT GAG CTA ATG CCG ATT CTT GAG A/3AmMO/ -3′ and complementary DNA (comp-DNA) oligomer with the sequence 5′- TCT CAA GAA TCG GCA TTA GCT CAA CTG TCA ACT CCT CTT T/3ThioMC3-D/ -3′. 200 μL of double-stranded DNA was prepared by mixing 20 μL of the HS-ssDNA with 22 μL of its complementary DNA from a stock solution of 100 μM. The mixture was kept in PCR, which was heated to a temperature of 372 K and allowed to cool to room temperature overnight. Thereafter, 70 μL of the solution was adsorbed on the TiO_2 electrodes.

Prior to adsorption of the dsDNA molecules, the electrodes were cleaned using ethanol and water. The surface was functionalized using terephtalic acid. To this end, 10 mM terephtalic acid solution was prepared in 10 mL of water and 100 μL of triethylamine. The electrodes were incubated in the terephtalic acid solution for 12 h, followed by rinsing with water. The previously functionalized surface for amide bond formation with the dsDNA was then activated by incubating the electrodes in a mixture of 60 mM N-hydrosuccinimide and 30 mM ethyl-N,N-dimethylcarbodiimide, which was dissolved in 0.8 M phosphate buffer. Electrodes were incubated for 15 h.

Finally, the dsDNA was adsorbed by keeping the electrodes for 24 h in a controlled humidified environment, after which the samples were rinsed with 0.4 M phosphate buffer and deionized water to remove any excess of DNA and salts. They were then blown dry using nitrogen gas. The electrodes were then immersed into the CdSe nanoparticle solution for at least 3 h.

Adsorption of CdSe Nanoparticles. CdSe NP (~7 nm diameter from MK Impex) was used in this study. The MKN-CdSe-T640 nanoparticle dispersion was mixed with toluene to afford a concentration of 22.5 mM. The functionalized TiO_2 electrodes were then incubated in the CdSe nanoparticle dispersions for at least 3 h to ensure the adsorption of CdSe NP to the S-terminal of the linker molecules. The electrodes were then rinsed thoroughly in toluene to remove the physisorbed NP and finally dried with nitrogen gas.

Photoelectrochemistry. To investigate the effects of modifying the TiO_2 electrodes with different linker molecules on the photoelectrochemical process, we performed Mott−Schottky impedance spectroscopy measurements. Photoelectrochemical measurements were performed in a three-electrode electrochemical cell, with Pt wire used as a counter electrode and with an Ag/AgCl (saturated KCl) reference electrode. A mixture of 0.35 M Na_2SO_3 and 0.25 M Na_2S aqueous solution (pH 9.5) was used as the electrolyte. The Na_2S sacrificial reagent plays the role of hole scavenger and is oxidized to S_2^{2-} to prevent the photocorrosion of CdSe.

To ensure efficient hydrogen production at the cathode, Na_2SO_3 was added to reduce disulfides back to sulfides, $S_2^{2-} + SO_3^{2-} = S^{2-} + S_2O_3^{2-}$, which has been shown to significantly increase the amount of hydrogen produced. A commercial Xe lamp with an intensity of 80 mW cm^{-2} was used to illuminate the photoelectrodes.

Two experimental configurations for hydrogen production, which are characterized by multiple electron transfer processes, were probed.[33] In the first, water is split to produce hydrogen and oxygen in an electrochemical cell in which a TiO_2 anode is coated with either chiral or achiral self-assembled molecular layers. In the second configuration, the same anode was used, but CdSe nanoparticles (NPs) were attached to the molecules and hydrogen was photogenerated using sacrificial electrolytes,[34] such as Na_2S and Na_2SO_3. Namely, here the sulfide is oxidized instead of oxygen via a multiple electron oxidation process. In both configurations, a three-electrode electrochemical cell was used, with a Pt wire as the cathode and Ag/AgCl (saturated KCl) as the reference electrode.

Table 1 presents the molecules studied in both experimental configurations. The chiral molecules are either oligopeptides, [L-(COOH)-(Ala-Aib)$_5$-NH-(CH$_2$)$_2$-SH and L-(COOH)-(Ala-Aib)$_7$-NH-(CH$_2$)$_2$-SH] having an α-helix structure, or 40 base-pair-long DNA (for details, see the Supporting Information). The molecules are bound to the titania surface through a carboxylic group, and in the second configuration CdSe nanoparticles are bound to the molecules through a thiol group. On this electrode, electrons are transferred from solution during oxidation, whereas on the counter electrode water is reduced to form hydrogen. To confirm the structure of the electrode, we conducted TEM measurements (see Figure S2 in the Supporting Information).

Table 1. Molecules Studied

| Al5 and Al7 | -(COOH)-(Ala-Aib)$_{5 \text{ or } 7}$-NH-(CH$_2$)$_2$-SH | |
MUA	SH-(CH$_2$)$_{10}$-COOH	
MPA	SH-(CH$_2$)$_2$-COOH	
4-MBA	p,SH-(C$_6$H$_4$)-COOH	
3-MBA	m,SH-(C$_6$H$_4$)-COOH	
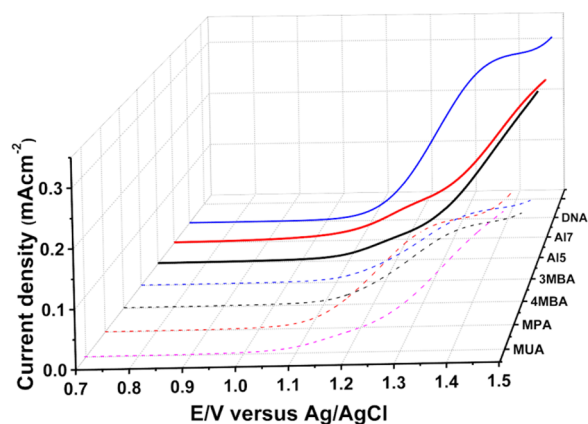
Figure 1. Current density as a function of the potential versus the Ag/AgCl electrode when the TiO$_2$ electrode is coated with self-assembled monolayers of either achiral (dashed lines) or chiral (solid lines) molecules. The experiments were performed in the dark.

In the first configuration (water splitting), the measurements were performed in a solution of 0.1 M Na$_2$SO$_4$, pH 6.32 at a scan rate of 50 mV/s.

Results and Disscusion. Figure 1 presents the current density as a function of the potential versus the Ag/AgCl electrode when the TiO$_2$ electrode is coated with self-assembled monolayers of either achiral (dashed lines) or chiral (solid lines) molecules. Here the experiments were performed in the dark. The scan was performed up to 1.5 V to avoid oxidation of the molecules and destruction of the organic monolayer. The gradients of the currents obtained with the chiral molecules at 1.5 V are much larger than those observed with the achiral

counterparts. It is important to realize that all achiral molecules are much shorter than the chiral ones, and several of them are highly conjugated (see Table 2). Hence, it is expected that the achiral molecules will conduct better and exhibit higher current. Interestingly, despite the larger molecular lengths of the chiral molecules, significantly lower threshold potentials for oxygen evolution, with a concomitant increase in the currents, with respect to the achiral molecules were observed. The extreme case is the 13 nm long DNA that exhibits high current despite being longer by about more than an order of magnitude than the MBA and MPA molecules. At a potential of 1.4 V, namely, an overpotential of <0.2 V, the current in the cells in which the anode is coated with chiral molecules is higher than that for cells containing the achiral molecules.

Figure 2 presents a cartoon of the photoelectrochemical cell and a qualitative scheme of the energy levels involved in the
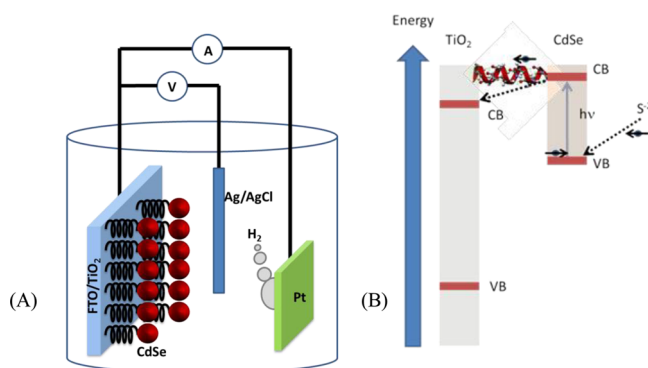

Figure 2. (A) Scheme of the photoelectrochemical cell used in the present study for water splitting. CdSe nanoparticles (red) are bound to the TiO$_2$ nanoparticles through chiral molecules. The TiO$_2$ nanoparticles are attached to the FTO conducting electrode. On the Pt electrode, the H$^+$ ions are reduced to form H$_2$. (B) Scheme of the electron transfer between the S^{2-} and the TiO$_2$ nanoparticles. Upon excitation of the CdSe nanoparticles, the excited electrons are transferred through the chiral molecules to TiO$_2$ (from there to the external circuit). This is a spin-specific electron transfer because the transfer through the chiral molecule is preferred for one spin over the other. Thus, the hole in the CdSe has a well-defined spin alignment; therefore, electrons with this spin will be transferred from the anions in the solution to CdSe.

photoexcitation/oxidation process occurring at the anode. The setup follows former studies in which CdSe nanoparticles (7 nm in diameter) were used as the photocatalyst.[35−37] On one side, TiO$_2$ particles are attached to a fluorine-doped tin oxide (FTO surface resistivity −7 Ohm/sq) conductive electrode.

Table 2. Molecules, Their Lengths, and the Potentials Measured in the Photoelectrochemical Cells Containing Them

	electrode	molecular length/Å	E_{app} (V) versus Ag/AgCl[a]	E_{fb}, flat band potential versus Ag/AgCl (V)	$E_{\text{app}} - E_{\text{fb}}$ (V)	η effective overpotential[b]
chiral	TiO$_2$/Al7	25	0.25	−0.83	1.08	0.17
	TiO$_2$/Al5	22	0.25	−0.68	0.93	0.02
	TiO$_2$/DNA	130	0.30	−0.61	0.91	0
achiral	TiO$_2$/MUA	14	0.70	−0.95	1.65	0.74
	TiO$_2$/MPA	6	0.70	−0.94	1.64	0.73
	TiO$_2$/4MBA	8	0.30	−1.11	1.41	0.5
	TiO$_2$/3MBA	7	0.30	−1.20	1.50	0.59

[a]Potential applied to the TiO$_2$ electrode vs the Ag/AgCl reference electrode to produce H$_2$ [b]Effective overpotential is calculated with respect to the $E_{\text{app}} - E_{\text{fb}}$ value of the TiO$_2$/DNA system.
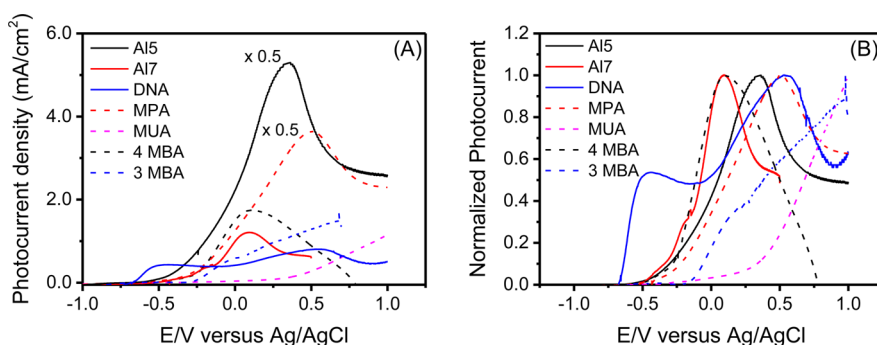
Figure 3. (A) Photocurrent density as a function of the potential versus the Ag/AgCl electrode. (B) Normalized photocurrent density as a function of the potential versus the Ag/AgCl electrode. The normalization was performed by taking the highest current in the range to be 1. The potential was not corrected to present the effective overpotential. The solid and dashed lines present cells with chiral and achiral molecules, respectively.

Our specific addition was the attachment of the CdSe nanoparticles to titania (TiO$_2$) by various molecular linkers including chiral ones. A mixture of Na$_2$SO$_3$ and Na$_2$S aqueous solution (pH 9.5) was used as the electrolyte. The Na$_2$S plays the role of both a hole scavenger and a sacrificial anodic electroactive species and is oxidized to S_2^{2-} and eventually to S_2 sulfur dimer ($^3\Sigma_g$ ground state),[38] thus preventing the photocorrosion of CdSe and enhancing the hydrogen production.[37] An Xe lamp with an intensity of 80 mW cm^{-2} was used for illuminating the photoelectrodes. Hydrogen gas evolution was monitored at various potentials using a potentiostat in the chronoamperometry mode under illumination. The evolved hydrogen gas was measured in an airtight H cell.

The cell operation is based on photoexcitation of the CdSe NP (see Figure 2B), while a potential is applied to the TiO$_2$ electrode versus the saturated Ag/AgCl electrode. A potential difference is established between the TiO$_2$ and the Pt electrodes. Upon photoexcitation, an electron is transferred from CdSe NP to the TiO$_2$ electrode, leaving a hole in the NP. Electrons from the sulfide oxidation process are then transferred to NP, and S_2^{2-} is produced. Thus, the cell overall current depends on the efficiency of the electron transfer from the photoexcited CdSe NP to the titania substrate. The molecules used as linkers between the NPs and titania and their respective lengths are listed in Tables 1 and 2.

To evaluate whether the electron-transfer efficiency controls the overall current of the photoelectrochemical cell, we measured room-temperature photoluminescence (PL) for the titania functionalized electrodes (i.e., titania functionalized with CdSe NPs attached via the linker listed in Table 1) using a green laser (wavelength of 514.5 nm) as an excitation source. The density of the NP on the surface was found to be the same, within 10% variation, for all of the different linkers (Figure S3 Supporting Information). The PL intensity from the adsorbed NP is inversely proportional to the efficiency of the fluorescence quenching due to electron transfer from the NP to the substrate. Indeed, the strongest signal is obtained for the long alkyl chain; the second in intensity is the signal from the electrode that is fabricated using the oligopeptide, and the weakest intensity results from the electrode with the shortest alkyl molecule (Figure S4, Supporting Information).

The electron transfer rate, k, is expressed by $k = k_0 e^{-\beta l}$, where β is the decay coefficient and l is the length of the molecule. For alkyl chains $\beta \approx 10$/nm; therefore, it is expected that the electron transfer rate in the short alkyl chain will be about an order of magnitude faster than that in the longer one,

as reflected in the PL intensity. For the oligopeptide used here, it was found that $\beta \approx 7$/nm,[39] and therefore, as expected, despite being longer than the MUA, electron transfer through the oligomer is more efficient; however, it is less efficient than the electron transfer through MPA.

To verify the spin selectivity of electron transmission through the oligopeptide, we conducted spin-specific conductive AFM measurements (see Figures S5–S8, Supporting Information) following the previously reported procedure.[40–42] The spin polarization measured is 18 ± 5, 25 ± 5, and 80 ± 5% for the Al5, Al7, and DNA samples, respectively. The polarization is defined as the difference in the current of the two spins over the sum. This amounts to ratios in transmission between the two spins that are 1:1.4, 1:1.7, and 1:6, respectively.

Figure 3 presents the photocurrent density versus the electric potential when measured through illuminated electrochemical cells. All chiral molecules feature a maximum photocurrent appearing at lower potentials (vs Ag/AgCl), as compared with the achiral molecules, in which the maximum photocurrent is observed at high potentials, with the exception of 4 MBA, which will be discussed later.

The actual potential required for driving the photoelectrochemical process depends on the flat-band potential (E_{fb}) of the semiconductor electrode.[43] This quantity is a measure of the potential that must be applied to the semiconductor, relative to some reference electrode, so that the bands remain flat as the interface is approached. Thus, the overpotential (η) is given by

$$\eta = E_{app} - E_{fb} - E_{th} \tag{1}$$

where E_{app} is the potential at which hydrogen appears and E_{th} is the thermodynamic value for the potential at which the reaction takes place. Table 2 presents the results obtained for all of the molecules. The values for E_{fb} were obtained from the Mott–Schottky plot, as measured from impedance spectroscopy (see Figure S9, Supporting Information). Here we refer to the effective overpotential, when E_{th} is taken as the value of $E_{app} - E_{fb}$ obtained with DNA molecules as a linker, which has the lowest value for $E_{app} - E_{fb}$. The 4MBA molecule is special because it is an exceptionally efficient electron conductor and has a highly negative flat band potential (E_{fb}), as discussed later. As shown in eq 1, if the value of E_{fb} is highly negative for the same overpotential, E_{app} is very low compared with other achiral molecules; however, Figure 3 confirms the general observation of high catalytic efficiency in cells with chiral molecules and especially the very low value for the potential needed in the case of DNA.

The effect of the chiral molecules on the hydrogen production is presented in Figure 4 and Table S1 in the
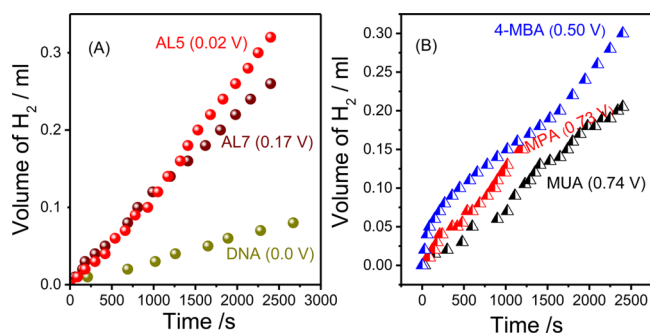
Figure 4. Hydrogen production as a function of time for (A) the chiral molecules and (B) for the achiral molecules. The potentials in the brackets refer to the overpotential as defined in Table 2. The measurements were conducted at E_{app} for each of the molecules.

Supporting Information. At low effective overpotential ($\eta < 0.5$ V vs Ag/AgCl), hydrogen is produced only when the working electrode includes the chiral molecules. At higher overpotentials, hydrogen is produced even when achiral molecules are used. Figure 4A shows that the overpotential is lower for the molecule with the higher spin selectivity, and thus the cell that includes DNA exhibits the lowest effective appearance potential.

The open-circuit potential (OCP) was measured in the dark and when the cell was illuminated. Besides 4MBA, the light had a relatively small effect on the OCP, as expected because most of the molecules are poor conductors. Because 4MBA is relatively a good conductor, it indeed shows a large effect of light (see Table S2 in the Supporting Information). In general, there is no significant difference between the OCP of the chiral and achiral molecules.

The spin polarization of electrons conducted through the chiral molecules is scaled by the molecular length. The yield of hydrogen production also depends on the molecular conduction, however in general, it decreases with increasing molecular length because of the increased resistance. Because all of the chiral molecules used are longer than the achiral ones, *the results clearly prove that the overpotential is dramatically reduced in the case of chiral molecules and that it is minimum for the molecule with the highest spin selectivity.*

Although a detailed mechanism for the formation of oxygen is not yet available, the experimental observations in the present study are consistent with the concept that the constraint of total spin conservation during the reaction process is responsible for the high overpotential observed in achiral systems. A plausible explanation to the result is that when electrons are conducted through chiral molecules the conduction is intrinsically spin-selective; therefore, the spins of the reacting atoms are coaligned. If the spin orientation of the two atoms is not the same, upon approaching each other, the atoms are situated on the repulsive singlet potential energy surface and therefore the reaction that forms oxygen molecules will have a barrier. Hence, spin alignment (*in the laboratory frame*) should reduce the barrier of the reaction.

In the second experimental configuration, upon photoexcitation of CdSe NP, a singlet state is formed in which the electrons in the ground state and excited state are anticorrelated; however, the spin orientation in the laboratory frame is isotropic. With chiral molecular linkers, electrons transferred through molecules from NP to titania are spin-dependent; namely, the isotropic distribution of the spin alignment, following photoexcitation, collapses to a well-defined spin orientation of the excited electrons. This is because only those electrons featuring one (up or down) spin state can be transferred efficiently through chiral molecules.[15] The electron in the ground state is therefore left with a spin orientation that is antiparallel to that of the transferred spin. Hence, when an electron with a well-defined spin alignment is transferred from NP, it leaves a hole in CdSe with the same spin direction. As a result, the electrons being transferred from the hole scavengers in solution are all transferred with the same spin alignment, leaving all atoms with the same unpaired spin direction in the laboratory frame. Therefore, the formation of the disulfide or the oxygen molecule can occur with a large cross-section. If spin alignment does not exist, as it occurs with nonchiral molecules, the formation of the ground-state molecules requires the two atoms (sulfur or oxygen) to be in proximity, so that the exchange interaction between the spins will be strong enough to define the spin alignment, whereas if the spins are already aligned, the reaction can take place at a larger distance. Of course some spin randomization occurs in NP, owing to spin–orbit coupling; however, the rates of the electron-transfer processes compete well with the spin relaxation time, which is on the order of picoseconds.[44]

The present work clearly supports the notion that electronic factors play a fundamental role in the origin of the overpotential. The results obtained with DNA and the oligopeptides are consistent with them being spin filters. With the very long DNA, in which the appearance potential is the lowest, the yield of hydrogen production is lower than that for the shorter oligomers. These results are consistent with a 40-base-pair DNA sequence being the best spin filter, as compared with the oligopeptides that have lower spin polarizations;[41] however, the electron transfer is more efficient through the shorter oligomers. This explains the high hydrogen production yield in cells in which the latter is used compared with a cell containing the DNA.

We suggest, based on the present study, that important contribution to the over potential observed in water splitting results from the barrier caused by the requirement that the atoms of the hole scavenger (oxygen or sulfur) have to be extremely close for the ground state of the molecule to form. By having "aligned spins", however, this requirement is relaxed and the barrier for the reaction is reduced; hence, the overpotential is reduced. Because key biochemical reactions in nature involve multiple electron reactions, like respiration, the results presented here indicate that spin selectivity may also be of paramount importance in other biological processes as well as in multiple electron processes used in industry, such as oxygen reduction.[45,46]

■ ASSOCIATED CONTENT

ⓢ Supporting Information

The Supporting Information is available free of charge on the ACS Publications website at DOI: 10.1021/acs.jpclett.5b02419.

> Details of the preparation of TiO₂ electrodes, the functionalization of the electrode by the linker molecules, and the adsorption of CdSe nanoparticles and structural characterization of the electrodes using SEM and TEM. Absorbance, room-temperature photoluminescence, and

electrochemical impedance spectroscopy data are also presented. Information is provided on spin selectivity in electron transmission through the oligopeptide. (PDF)

■ AUTHOR INFORMATION

Corresponding Author
*E-mail: ron.naaman@weizmann.ac.il.

Notes
The authors declare no competing financial interest.

■ ACKNOWLEDGMENTS

■ REFERENCES

(1) Han, Z.; Eisenberg, R. Fuel from Water: The Photochemical Generation of Hydrogen from Water. *Acc. Chem. Res.* **2014**, *47*, 2537−2544.

(2) Meyer, T. J. Chemical Approaches to Artificial Photosynthesis. *Acc. Chem. Res.* **1989**, *22*, 163−170.

(3) Bard, A. J.; Fox, M. A. Artificial Photosynthesis: Solar Splitting of Water to Hydrogen and Oxygen. *Acc. Chem. Res.* **1995**, *28*, 141−145.

(4) Blankenship, R. E.; Tiede, D. M.; Barber, J.; Brudvig, G. W.; Fleming, G.; Ghirardi, M.; Gunner, M. R.; Junge, W.; Kramer, D. M.; Melis, A.; et al. Comparing Photosynthetic and Photovoltaic Efficiencies and Recognizing the Potential for Improvement. *Science* **2011**, *332*, 805−809.

(5) Tachibana, Y.; Vayssieres, L.; Durrant, J. R. Artificial photosynthesis for Solar Water Splitting. *Nat. Photonics* **2012**, *6*, 511−518.

(6) Reece, S. Y.; Hamel, J. A.; Sung, K.; Jarvi, T. D.; Esswein, A. J.; Pijpers, J. J. H.; Nocera, D. G. Wireless Solar Water Splitting Using Silicon-Based Semiconductors and Earth-Abundant Catalysts. *Science* **2011**, *334*, 645−648.

(7) Yuhas, B. D.; Smeigh, A. L.; Douvalis, A. P.; Wasielewski, M. R.; Kanatzidis, M. G. Photocatalytic Hydrogen Evolution from FeMoS-Based Biomimetic Chalcogels. *J. Am. Chem. Soc.* **2012**, *134*, 10353−10356.

(8) Gray, H. B. Powering the Planet with Solar Fuel. *Nat. Chem.* **2009**, *1*, 7.

(9) Sivula, K.; Le Formal, F.; Grätzel, M. Solar Water Splitting: Progress Using Hematite (α-Fe_2O_3) Photoelectrodes. *ChemSusChem* **2011**, *4*, 432−449.

(10) Brillet, J.; Cornuz, M.; Le Formal, F.; Yum, J. H.; Gratzel, M.; Sivula, K. Examining Architectures of Photoanode-photovoltaic Tandem Cells for Solar Water Splitting. *J. Mater. Res.* **2010**, *25*, 17−24.

(11) Mayer, M. T.; Du, C.; Wang, D. Hematite/Si Nanowire Dual-Absorber System for Photoelectrochemical Water Splitting at Low Applied Potentials. *J. Am. Chem. Soc.* **2012**, *134*, 12406−12409.

(12) Chretien, S.; Metiu, H. O_2 Evolution on a Clean Partially Reduced Rutile TiO_2 (110) Surface and on the Same Surface Precovered with Au_1 and Au_2: The importance of Spin Conservation. *J. Chem. Phys.* **2008**, *129*, 074705−074716.

(13) Torun, E.; Fang, C. M.; de Wijs, G. A.; de Groot, R. A. Role of Magnetism in Catalysis: RuO_2 (110) Surface. *J. Phys. Chem. C* **2013**, *117*, 6353−6357.

(14) Naaman, R.; Waldeck, D. H. Chiral-Induced Spin Selectivity Effect. *J. Phys. Chem. Lett.* **2012**, *3*, 2178−2187.

(15) Naaman, R.; Waldeck, D. H. Spintronics and Chirality: Spin Selectivity in Electron Transport through Chiral Molecules. *Annu. Rev. Phys. Chem.* **2015**, *66*, 263−281.

(16) Siegbahn, P. E. M.; Crabtree, R. H. Manganese Oxyl Radical Intermediates and O-O Bond Formation in Photosynthetic Oxygen Evolution and a Proposed Role for the Calcium Cofactor in Photosystem II. *J. Am. Chem. Soc.* **1999**, *121*, 117−127.

(17) McEvoy, J. P.; Gascon, J. A.; Batista, V. S.; Brudvig, G. W. The mechanism of photosynthetic Water Splitting. *Photochem. Photobiol. Sci.* **2005**, *4*, 940−949.

(18) (a) Tommos, C.; Tang, X. − S.; Warncke, K.; Hoganson, C. W.; Styring, S.; McCracken, J.; Diner, B. A.; Babcock, G. T. Spin-Density Distribution, Conformation, and Hydrogen Bonding of the Redox-Active Tyrosine Y_z in Photosystem I1 from Multiple Electron Magnetic-Resonance Spectroscopies: Implications for Photosynthetic Oxygen Evolution. *J. Am. Chem. Soc.* **1995**, *117*, 10325−10335.

(19) Rivalta, I.; Yang, K. R.; Brudvig, G. W.; Batista, V. S. Triplet Oxygen Evolution Catalyzed by a Biomimetic Oxomanganese Complex: Functional Role of the Carboxylate Buffer. *ACS Catal.* **2015**, *S*, 2384−2390.

(20) Yamaguchi, K.; Yamanaka, S.; Isobe, H.; Tanaka, K.; Ueyama, N. Spin Hamiltonian Models for Artificial and Native Water Splitting Systems Revealed by Hybrid DFT Calculations. Oxygen Activation by High-Valent Mn and Ru Ions. *Int. J. Quantum Chem.* **2012**, *112*, 3849−3866.

(21) Yang, X.; Baik, M. H. The Mechanism of Water Oxidation Catalysis Promoted by $[tpyRu(IV)=O]_2L^{3+}$: A Computational Study. *J. Am. Chem. Soc.* **2008**, *130*, 16231−16240.

(22) Bozoglian, F.; Romain, S.; Ertem, M. Z.; Todorova, K. T.; Sens, C.; Mola, J.; Rodríguez, M.; Romero, I.; Benet-Buchholz, J.; Fontrodona, X.; et al. The Ru-Hbpp Water Oxidation Catalyst. *J. Am. Chem. Soc.* **2009**, *131*, 15176−15187.

(23) Jaque, P.; Marenich, A. V.; Cramer, C. J.; Truhlar, D. G. Computational Electrochemistry: The Aqueous $Ru^{3+}|Ru^{2+}$ Reduction Potential. *J. Phys. Chem. C* **2007**, *111*, 5783−5799.

(24) Carmeli, I.; Kumar, K. S.; Heifler, O.; Carmeli, C.; Naaman, R. Spin Selectivity in Electron Transfer in Photosystem I. *Angew. Chem., Int. Ed.* **2014**, *53*, 8953−8958.

(25) Salant, A.; Shalom, M.; Hod, I.; Faust, A.; Zaban, A.; Banin, U. Quantum Dot Sensitized Solar Cells with Improved Efficiency Prepared Using Electrophoretic Deposition. *ACS Nano* **2010**, *4*, 5962−5968.

(26) Li, X.; Qiu, Y.; Wang, S.; Lu, S.; Gruar, R. I.; Zhang, X.; Darr, J. A.; He, T. Electrophoretically Deposited TiO_2 Compact Layers using aqueous suspension for dye-sensitized solar cells. *Phys. Chem. Chem. Phys.* **2013**, *15*, 14729−14735.

(27) Yum, J.-H.; Kim, S.-S.; Kim, D.-Y.; Sung, Y.-E. Electrophoretically Deposited TiO_2 Photo-electrodes for use in Flexible Dye-sensitized Solar Cells. *J. Photochem. Photobiol., A* **2005**, *173*, 1−6.

(28) Fukada, Y.; Nagarajan, N.; Mekky, W.; Bao, Y.; Kim, H.-S.; Nicholson, P. S. Electrophoretic Deposition-mechanisms, Myths and Materials. *J. Mater. Sci.* **2004**, *39*, 787−801.

(29) Besra, L.; Liu, M. A Review on Fundamentals and Applications of Electrophoretic Deposition (EPD). *Prog. Mater. Sci.* **2007**, *52*, 1−61.

(30) Mann, J. R.; Watson, D. Adsorption of CdSe Nanoparticles to Thiolated TiO_2 Surfaces: Influence of Interlayer Disulfide Formation on CdSe Surface coverage. *Langmuir* **2007**, *23*, 10924−10928.

(31) Chen, J.; Franking, R.; Ruther, R. E.; Tan, Y.; He, X.; Hogendoorn, R. S.; Hamers, R. J. Formation of Molecular Monolayers on TiO_2 Surfaces: A Surface Analogue of Williamson Ether Synthesis. *Langmuir* **2011**, *27*, 6879−6889.

(32) Titheridge, D. J.; Barteau, M. A.; Idriss, H. Reaction of Acrylic Acid on TiO_2 (001) Single Crystal Surfaces. Evidence of Different Pathways for Vinyl and Carboxyl Groups. *Langmuir* **2001**, *17*, 2120−2128.

(33) Bak, T.; Nowotny, J.; Rekas, M.; Sorrell, C. C. Photo-electrochemical Hydrogen Generation from Water Using Solar Energy. Materials-related aspects. *Int. J. Hydrogen Energy* **2002**, *27*, 991−1022.

(34) Rao, N. N.; Dube, S. Photoelectrochemical Generation of Hydrogen Using Organic Pollutants in Water as Sacrificial Electron Donors. *Int. J. Hydrogen Energy* **1996**, *21*, 95−98.

(35) Frame, F. A.; Carroll, E. C.; Larsen, D. S.; Sarahan, M.; Browning, N. D.; Osterloh, F. E. First Demonstration of CdSe as a Photocatalyst for Hydrogen Evolution from Water under UV and Visible Light. *Chem. Commun.* **2008**, 2206−2208.

(36) Das, A.; Han, Z.; Haghighi, M. G.; Eisenberg, R. Photogeneration of Hydrogen from Water Using CdSe Nanocrystals Demonstrating the Importance of Surface Exchange. *Proc. Natl. Acad. Sci. U. S. A.* **2013**, *110*, 16716−16723.

(37) Hensel, J.; Wang, G.; Li, Y.; Zhang, J. Z. Synergistic Effect of CdSe Quantum Dot Sensitization and Nitrogen Doping of TiO_2 Nanostructures for Photoelectrochemical Solar Hydrogen Generation. *Nano Lett.* **2010**, *10*, 478−483.

(38) Uzunova, E. L.; Mikosch, H. Electronic, Magnetic Structure and Water Splitting Reactivity of the Iron-sulfur Dimers and Their Hexacarbonyl Complexes. *J. Chem. Phys.* **2014**, *141*, 044307−044313.

(39) Sek, S.; Tolak, A.; Misicka, A.; Palys, B.; Bilewicz, R. Asymmetry of Electron Transmission through Monolayers of Helical Polyalanine Adsorbed on Gold Surfaces. *J. Phys. Chem. B* **2005**, *109*, 18433−18438.

(40) Nogues, C.; Cohen, S. R.; Daube, S. S.; Naaman, R. Electrical Properties of Short DNA Oligomers Characterized by Conducting Atomic Force Microscopy. *Phys. Chem. Chem. Phys.* **2004**, *6*, 4459−4466.

(41) Xie, Z.; Markus, T. Z.; Cohen, S. R.; Vager, Z.; Gutierrez, R.; Naaman, R. Spin Specific Electron Conduction through DNA Oligomers. *Nano Lett.* **2011**, *11*, 4652−4655.

(42) Kettner, M.; Göhler, B.; Zacharias, H.; Mishra, D.; Kiran, V.; Naaman, R.; Fontanesi, C.; Waldeck, D. H.; Sȩk, S.; Pawłowski, J.; et al. Spin Filtering in Electron Transport through Chiral Oligopeptides. *J. Phys. Chem. C* **2015**, *119*, 14542−14547.

(43) Bard, A. J.; Faulkner, L. R. *Electrochemical Methods Fundamentals and Applications*; John Wiley & Sons Inc., 2001; Ch. 18.

(44) Huxter, V. M.; Kim, J.; Lo, S. S.; Lee, A.; Nair, P. S.; Scholes, G. D. Spin Relaxation in Zinc Blende and Wurtzite CdSe Quantum Dots. *Chem. Phys. Lett.* **2010**, *491*, 187−192.

(45) Bott, A. W. The Study of Multiple Electron Transfer Reactions by Cyclic Voltammetry. *Curr. Sep.* **1997**, *16*, 61−66.

(46) Song, C.; Zhang, J. *Electrocatalytic Oxygen Reduction Reaction*; Springer: London, 2008; pp 89−134.